Rapid reductions and millennial-scale variability in Nordic Seas sea ice cover during abrupt glacial climate changes

Henrik Sadatzki[a,b,c,1], Niccolò Maffezzoli[d,e,f], Trond M. Dokken[b,g], Margit H. Simon[b,g], Sarah M. P. Berben[a,b], Kirsten Fahl[c], Helle A. Kjær[d], Andrea Spolaor[e,f], Ruediger Stein[c,h], Paul Vallelonga[d,i], Bo M. Vinther[d], and Eystein Jansen[a,b,g]

[a]Department of Earth Science, University of Bergen, 5007 Bergen, Norway; [b]Bjerknes Centre for Climate Research, 5007 Bergen, Norway; [c]Marine Geology Section, Alfred Wegener Institute Helmholtz Centre for Polar and Marine Research, 27568 Bremerhaven, Germany; [d]Centre for Ice and Climate, Niels Bohr Institute, University of Copenhagen, 2100 Copenhagen, Denmark; [e]Department of Environmental Sciences, Informatics and Statistics, Ca' Foscari University of Venice, 30170 Venice Mestre, Italy; [f]Institute of Polar Science–National Research Council of Italy, (I) 30172 Venezia-Mestre (VE), Italy; [g]Climate, Norwegian Research Centre AS (NORCE), 5007 Bergen, Norway; [h]MARUM Center for Marine Environmental Sciences and Faculty of Geosciences, University of Bremen, 28334 Bremen, Germany; and [i]Oceans Institute, The University of Western Australia, Crawley, WA 6009, Australia

Edited by Örjan Gustafsson, Stockholm University, Stockholm, Sweden, and accepted by Editorial Board Member Mark Thiemens September 23, 2020 (received for review March 28, 2020)

Constraining the past sea ice variability in the Nordic Seas is critical for a comprehensive understanding of the abrupt Dansgaard-Oeschger (D-O) climate changes during the last glacial. Here we present unprecedentedly detailed sea ice proxy evidence from two Norwegian Sea sediment cores and an East Greenland ice core to resolve and constrain sea ice variations during four D-O events between 32 and 41 ka. Our independent sea ice records consistently reveal a millennial-scale variability and threshold response between an extensive seasonal sea ice cover in the Nordic Seas during cold stadials and reduced seasonal sea ice conditions during warmer interstadials. They document substantial and rapid sea ice reductions that may have happened within 250 y or less, concomitant with reinvigoration of deep convection in the Nordic Seas and the abrupt warming transitions in Greenland. Our empirical evidence thus underpins the cardinal role of rapid sea ice decline and related feedbacks to trigger abrupt and large-amplitude climate change of the glacial D-O events.

sea ice | Nordic Seas | Dansgaard–Oeschger events | abrupt climate change

Sea ice is a critical component of the global climate system as it affects Earth's albedo, phytoplankton productivity, ocean-atmosphere heat and gas exchange, and ocean circulation (1). Rapid sea ice retreat, as observed in the modern Arctic Ocean, exerts important climate feedbacks that may lead to an accelerated climate warming at northern high latitudes (2). While many climate models have difficulties in reproducing the currently observed Arctic sea ice decline (3), the rates of ongoing atmospheric warming in some Arctic regions are already comparable with those of prominent abrupt climate changes that occurred during the last glacial period (4). The latter are referred to as Dansgaard–Oeschger (D-O) climate events and known from Greenland ice core records as abrupt shifts between cold Greenland stadials (GS) and warmer Greenland interstadials (GI) occurring repeatedly ∼10–110 ka (5, 6). The millennial-scale glacial climate variability was a global phenomenon with different characteristics in the northern and southern hemispheres, but the most striking feature of the D-O events is an extremely abrupt climate transition that includes an atmospheric warming of 5–16.5 °C over the Greenland ice sheet happening in just a few decades (7). Analogous to the modern and future sea ice retreat and resulting warming in the Arctic, the abrupt D-O climate transitions are widely believed to have been amplified by rapid sea ice retreat in the Nordic Seas (8–15).

Today, the Nordic Seas are largely ice-free, and warm Atlantic surface waters flow into the Norwegian Sea as far north as Svalbard at ∼80°N (Fig. 1), where the Arctic sea ice cover is being eroded, in particular in the Barents Sea. The warm Atlantic surface waters release heat to the atmosphere as it flows northward, which is accompanied by convective intermediate and deep-water formation between Norway and Greenland, feeding the lower limb of the Atlantic Meridional Overturning Circulation (AMOC) (16). A portion of the Atlantic waters continues flowing into the stratified Arctic Ocean as subsurface waters (17). While the pattern of ocean circulation during GI was fairly comparable to that today, proxy data indicate that the glacial Nordic Seas exhibited a stable surface stratification during GS, similar to the modern Arctic Ocean (13, 18). The AMOC and associated northward surface heat transport into the Nordic Seas were weakened during GS, with most extreme weakening related to Heinrich events signified by massive iceberg discharges to the North Atlantic (19, 20). Intermediate and deep waters in the stadial Nordic Seas were 2–4 °C warmer as compared with GI or modern conditions, resulting from a stable halocline and reduced open-ocean convection (21, 22). Contemporaneously, an extended sea ice cover reaching at least as

Significance

The last glacial period was marked by abrupt, high-amplitude Greenland warming events, known as Dansgaard–Oeschger (D-O) events, which were likely linked with Nordic Seas sea ice retreat. We reconstruct the sea ice variability during four D-O events ∼32–41 ka with unprecedented spatial representation and rigorous temporal constraints, using proxy records from two Norwegian Sea sediment cores and an East Greenland ice core. Our records reveal millennial-scale variations between extended sea ice conditions and reduced seasonal sea ice conditions, with rapid sea ice reductions at the onset of D-O events. Our findings imply that rapid sea ice reduction amplified ocean-atmosphere processes causing the abrupt D-O climate transitions, providing constraints for model simulations of abrupt climate changes and their mechanisms.

Author contributions: H.S., N.M., T.M.D., P.V., B.M.V., and E.J. designed research; H.S., N.M., K.F., and A.S. performed research; H.S., N.M., T.M.D., M.H.S., S.M.P.B., K.F., H.A.K., A.S., R.S., P.V., B.M.V., and E.J. analyzed data; and H.S., N.M., M.H.S., A.S., P.V., and E.J. wrote the paper.

The authors declare no competing interest.

This article is a PNAS Direct Submission. Ö.G. is a guest editor invited by the Editorial Board.

[1]To whom correspondence may be addressed. Email: henrik.sadatzki@awi.de.

This article contains supporting information online at https://www.pnas.org/lookup/suppl/doi:10.1073/pnas.2005849117/-/DCSupplemental.

First published November 9, 2020.

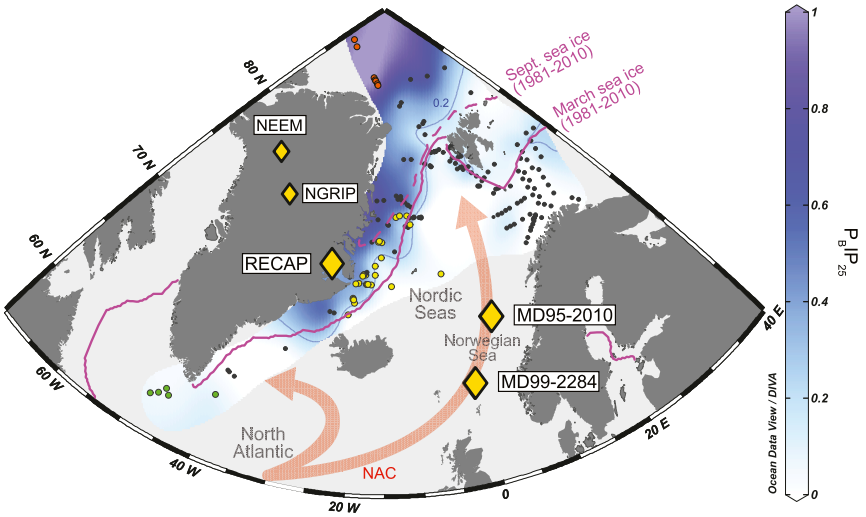

Fig. 1. Core sites and regional context of the study area. Yellow diamonds mark the core sites investigated in this study. The map shows the core-top P_BIP_{25} distribution (42, 43, 63), illustrating the great potential of the biomarker approach for sea ice reconstruction. Orange, yellow, and green dots mark core-top sites north, east, and south of Greenland, respectively, data of which are investigated in this study. Small black dots indicate locations of published core-top data. Purple lines mark the modern sea ice extent during September (dashed) and March (solid), averaged between A.D. 1981 and 2010 (https://nsidc.org/; ref. 64). The thin blue line shows the P_BIP_{25} = 0.2 isoline, representing best the modern winter/spring sea ice extent. Red arrows illustrate the warm and saline North Atlantic Current (NAC). The map was produced with Ocean Data View software (65).

far south as the Greenland–Scotland Ridge at ∼60°N insulated the high-latitude atmosphere from the deep oceanic heat reservoir (23, 24). Model simulations support a subsurface warming scenario under extended sea ice during GS (22, 25, 26) and suggest that a rapid removal of the sea ice cover might have caused the abrupt and high-amplitude D-O climate warming (11, 12, 14, 15).

Although there is some evidence of millennial-scale sea ice fluctuations during the last glacial, the few available sea ice proxy records (23, 24, 27–31) are mostly restricted to the southern Norwegian Sea and the Arctic Ocean, often have a limited temporal resolution, and partly reflect opposing trends regarding stadial–interstadial sea ice changes depending on the proxies used. Here we present high-resolution sea ice biomarker records from two key sites that form a North–South transect within the Atlantic inflow region in the Norwegian Sea and are thus ideally suited to record spatiotemporal shifts in sea ice cover in both the entrance and the interior of the ocean basin, oceanic fronts, and Atlantic water inflow during the last glacial (Fig. 1). Furthermore, we combine these marine sea ice proxy records with an independent sea ice record based on bromine-enrichment (Br_{enr}) values from an East Greenland ice core, which significantly enhances the spatial coverage, the robustness of results, and temporal constraint of the sea ice reconstruction. We focus on five representative glacial D-O cycles between 32 and 41 ka, which comprise long- and short-lasting GI as well as several GS, one of which includes Heinrich Event 4. The application of the cryptotephra-based chronological constraints provides a level of robustness as to the timing, duration, and nature of the events unfolding during abrupt climate changes. Our study provides robust empirical evidence that resolves rapid and widespread sea ice retreat in the Nordic Seas and its role in initiating and amplifying the abrupt climate change of the glacial D-O events.

Results

Core Sites, Chronology, and Sea Ice Biomarkers. Our marine biomarker proxy records are based on new data from core MD95-2010 (66° 41.05′ N, 04° 33.97′ E; 1,226 m water depth) and published data (24) from core MD99-2284 (62° 22.48′ N, 0° 58.81′ W; 1,500-m water depth) retrieved from the central and southern Norwegian Sea, respectively (Fig. 1). We complement our marine sea ice proxy records with a Br_{enr}-based sea ice reconstruction from the RECAP (Renland Ice Cap Project) ice core, drilled in East Greenland (71° 18.30′ N, 26° 43.38′ W; 2,315-m elevation). The modern source area for marine aerosols arriving at the RECAP ice core site comprises the northern North Atlantic and Nordic Seas at ∼50–85°N (32), including sites MD95-2010 and MD99-2284 (*SI Appendix*, Fig. S1). Sea ice records from both the sediment cores and the RECAP ice core can thus be expected to similarly reflect the glacial sea ice variability in the Nordic Seas, providing local and larger-scale signals, respectively.

A near-surface temperature record of core MD99-2284 based on planktic foraminifera census counts reveals millennial-scale temperature variations over the course of the D-O cycles at 32–41 ka (13). Comprehensive cryptotephra evidence from the same core demonstrates that rapid 2–3 °C warming transitions in the southern Norwegian Sea were coeval with the abrupt D-O warming over Greenland (33). Accordingly, the age model of MD99-2284 is based on alignment of near-surface temperature signals and D-O climate transitions, independently verified and constrained by four distinct cryptotephra layers that were identified before and after the GS6-GI5 transition as well as during GI6 and GI8 in both core MD99-2284 and the NGRIP (North Greenland Ice Core Project) ice core with a consistent geochemistry (33) (*SI Appendix*, *Materials and Methods* and Fig. S2). Moreover, the glacial sediment sections in both cores MD95-2010 and MD99-2284 reveal a very consistent variability in anhysteretic remanent magnetization (ARM), reflecting deep ocean circulation changes in the Nordic Seas (13, 34, 35), which closely resemble the D-O climate fluctuations recorded by the $\delta^{18}O$ of the NGRIP ice core. This enables development of an age model for core MD95-2010 by stratigraphic alignment of its ARM record to that of MD99-2284 and the $\delta^{18}O$ of the NGRIP ice core (*SI Appendix*, *Materials and Methods* and Fig. S2). Thereby, our sedimentary sea ice records are placed on the Greenland ice core chronology GICC05 (36) and can thus be directly compared with the RECAP sea ice record, which also has been transferred to the GICC05 chronology by alignment of the RECAP dust record to NGRIP $\delta^{18}O$ (37) (*SI Appendix*, *Materials and Methods* and Fig. S2). Accordingly, our sea ice records cover four D-O climate cycles between 32 and 41 ka (before 2000 CE = b2k) with a temporal resolution of 35–330 y for MD95-2010 and

10–120 y for MD99-2284, a resolution that is suitable for a detailed investigation of millennial-scale variability.

To reconstruct the glacial sea ice cover in the Norwegian Sea, we use a suite of molecular biomarkers analyzed in cores MD95-2010 and MD99-2284 as well as in 41 core tops from north, east, and south of Greenland (*SI Appendix*, *Materials and Methods*). In particular, we employ the sea ice biomarker IP_{25}, a highly branched isoprenoid (HBI) monoene produced by sea ice diatoms during spring, which allows tracing the occurrence of seasonal sea ice (38) (*SI Appendix*, Fig. S3). To further characterize the sea ice seasonality, we additionally use the abundance of an HBI triene (HBI-III) that occurs under ice-free conditions and in peak concentrations in regions influenced by the retreating sea ice edge or marginal ice zone (39, 40). To trace enhanced open-ocean conditions, we use increased abundances of the phytoplankton biomarkers brassicasterol, mainly produced by open-water diatoms (41). Moreover, we combine paired IP_{25} and brassicasterol (or HBI-III) signals in the so-called phytoplankton-IP_{25} (PIP_{25}) index, which allows solving the ambiguity regarding low/absent IP_{25} reflecting either perennial sea ice cover or absent sea ice and thus enables semiquantitative sea ice reconstructions (40, 42) (*SI Appendix*, *Materials and Methods*). Core-top PIP_{25} values clearly reflect the modern Arctic and sub-Arctic sea ice cover, illustrating the great potential of the sea ice biomarker approach (40, 42, 43) (Fig. 1 and *SI Appendix*, Fig. S3).

Millennial-Scale Sea Ice Variability in the Glacial Norwegian Sea. The down-core records of MD95-2010 from the central Norwegian Sea reveal IP_{25} in variable concentrations in all samples investigated and pronounced millennial-scale variations in brassicasterol and HBI-III, in concert with the GS-GI climate variability reflected by the NGRIP $\delta^{18}O$ (Fig. 2*A*). This suggests that sea ice was present in the central Norwegian Sea during the 32–41-ka interval and that seasonal sea ice versus open-water conditions varied over the course of the D-O climate cycles. MD95-2010 biomarker values show two main clusters in brassicasterol–IP_{25} and HBI-III–IP_{25} cross-plots, corresponding to stadial values (where $PIP_{25} > 0.5$) and interstadial values (where $PIP_{25} < 0.5$) (Fig. 2 *B* and *C*). Individual biomarker concentrations (normalized to total organic carbon content) and PIP_{25} values observed for the glacial millennial-scale variability in MD95-2010 are similar to those observed for the core-top samples that were investigated in this study using the same analytical procedure (*SI Appendix*, *Materials and Methods*), indicating sea ice conditions in the same range as in the modern (sub)Arctic. This allows us to interpret the stadial and interstadial sea ice conditions in the Norwegian Sea in view of the different sea ice conditions observed today at the northern, eastern, and southern Greenland margins (Fig. 1).

GS intervals in MD95-2010 are characterized by near-zero concentrations of brassicasterol and HBI-III, suggesting a strongly

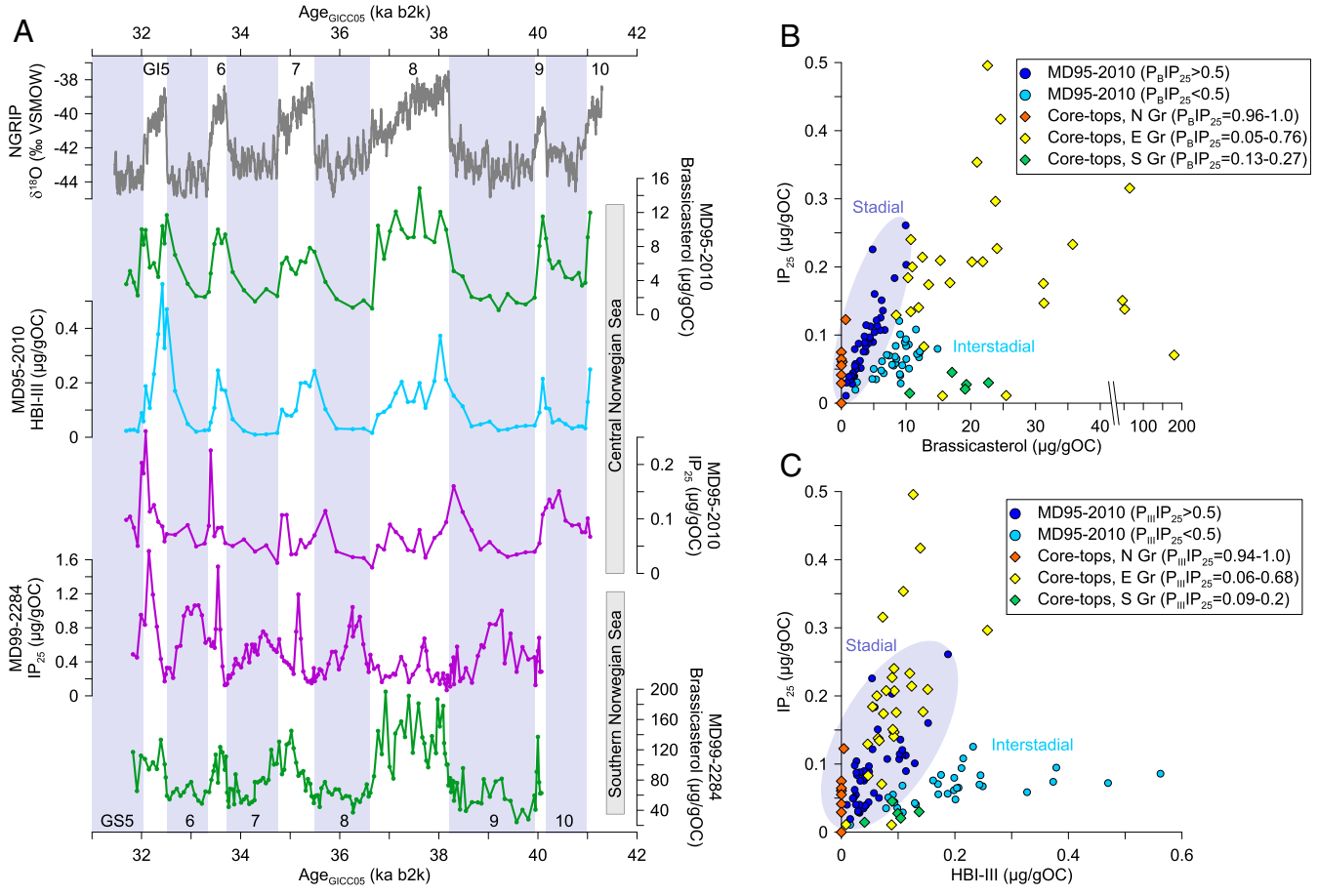

Fig. 2. Biomarker proxy records of Norwegian Sea sediment cores as well as arctic and subarctic core-top data. (*A*) From top to bottom: $\delta^{18}O$ of the NGRIP ice core plotted as 11-point running average (6); MD95-2010 records of brassicasterol (green), HBI-III (light blue), and IP_{25} (purple); MD99-2284 records of brassicasterol (green) and IP_{25} (purple) (24). All records are plotted on the GICC05 b2k timescale (36). GI are numbered at the top, GS (shaded bars) at the bottom. *B* and *C* show cross-plots of brassicasterol–IP_{25} and HBI-III–IP_{25}, respectively, for data from core MD95-2010 and core tops from north, east, and south of Greenland. MD95-2010 data are color-coded according to the resulting PIP_{25} value being >0.5 or <0.5, corresponding largely to stadial and interstadial values, respectively. Core-top data points are color-coded according to their location, and ranges of resulting PIP_{25} values are given.

reduced phytoplankton production. IP_{25} is also lowered during GS, except for later halves of GS8, GS9, and GS10, which points to a diminished spring ice algae production (Fig. 2*A*). These stadial biomarker signals in MD95-2010 are similar to those observed in our core tops from the largely ice-covered northern and proximal eastern Greenland margins (Fig. 2 *B* and *C*). Hence, we infer an extended (near-) perennial sea ice cover in the central Norwegian Sea during GS. By contrast, GI intervals in MD95-2010 are marked by elevated brassicasterol and HBI-III concentrations, which roughly quadrupled compared to GS (Fig. 2*A*). This indicates an enhanced open-water phytoplankton production near the marginal ice zone, supported by increased variable IP_{25} (39, 40, 42). Interstadial biomarker signals in MD95-2010 resemble those found in core tops from the eastern and southern Greenland margins near the maximum winter sea ice extent (Fig. 2 *B* and *C*). Our results thus suggest a reduced seasonal sea ice cover for the central Norwegian Sea during GI.

Differences between the IP_{25} records of MD95-2010 and MD99-2284 reveal insights into spatiotemporal shifts in the glacial sea ice edge position, while parallel brassicasterol variations at both sites consistently reflect a large-scale stimulation (reduction) of the phytoplankton production during GI (GS). When IP_{25} is lowered at site MD95-2010, it is increased at MD99-2284 at the onsets and in early parts of GS, suggesting a (near-) perennial sea ice cover in the central Norwegian Sea and an extended seasonal sea ice cover in the southern Norwegian Sea (24). As IP_{25} decreases at site MD99-2284 in the proceeding GS or its terminal phase, it increases at site MD95-2010 during latest GS9 and GS8 (Fig. 2*A*). This indicates a northward shift of the sea ice edge/marginal ice zone preceding GS-GI transitions

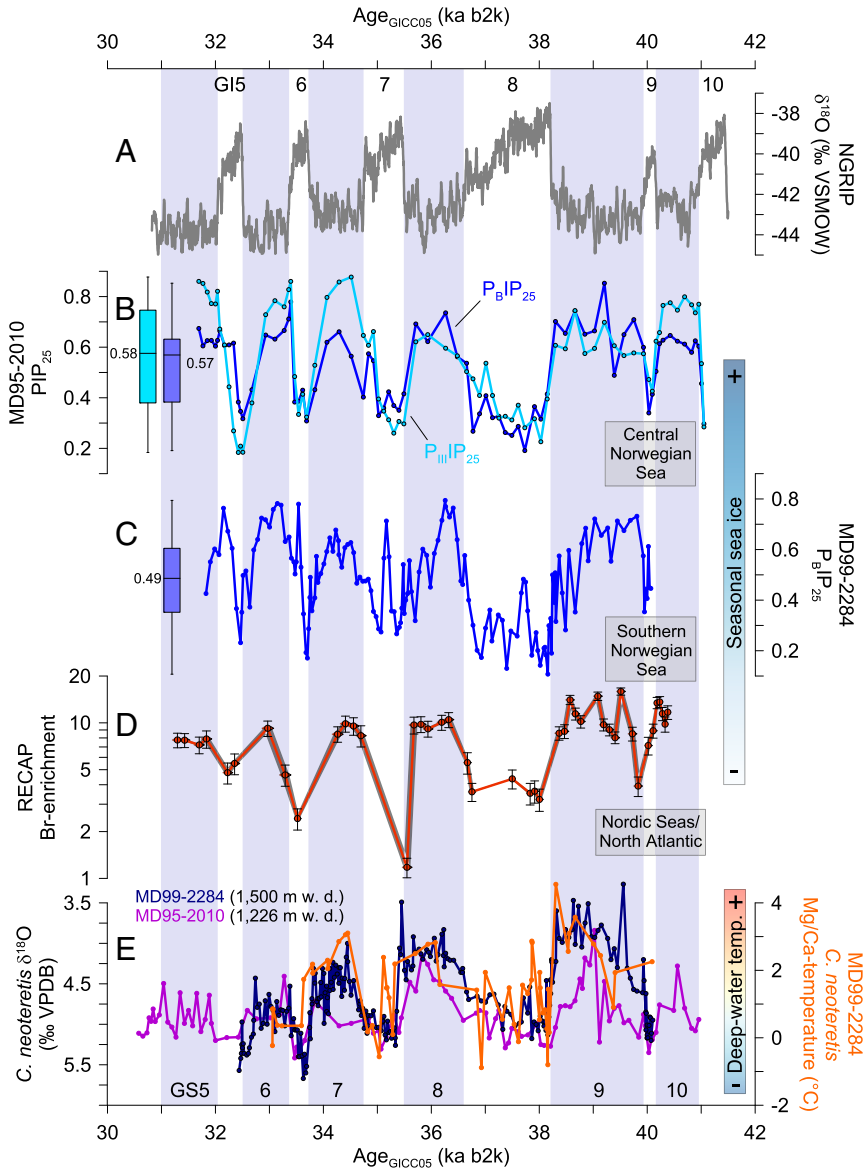

Fig. 3. Sea ice variability in the Nordic Seas based on sediment and ice core records covering ~32–41 ka. (*A*) δ^{18}O of the NGRIP ice core plotted as 11-point running average (6). (*B*) P_BIP_{25} (blue) and $P_{III}IP_{25}$ (light blue) of MD95-2010. (*C*) P_BIP_{25} of MD99-2284 (blue) (24). Boxes in *B* and *C* represent the interquartile range (IQR) of all P_BIP_{25} (blue) and $P_{III}IP_{25}$ values (light blue), with the whiskers being 1.5 × IQR and the medians being displayed. (*D*) Br_{enr} of the RECAP ice core (red). (*E*) Benthic foraminiferal δ^{18}O of MD99-2284 (13) (dark blue) and MD95-2010 (35) (purple) as well as deep-water temperature estimates based on benthic foraminiferal Mg/Ca of MD99-2284 (22) (orange). All records are plotted on the GICC05 b2k timescale (36). GI) are numbered at the top, GS (shaded bars) at the bottom.

(24). This initial sea ice reduction, however, is not resolved for the GS7-GI6 and GS6-GI5 transitions in core MD95-2010, either because of a too low temporal resolution of the record or because the sea ice edge did not shift as far north as the core site during terminal GS7 and GS6. Maximum open-ocean conditions in the Norwegian Sea were reached at the onset of GI, when the marginal ice zone was located near site MD95-2010. Yet, both cores reveal IP_{25} evidence of seasonal sea ice occurrence during GI. Successive peaks in HBI-III and IP_{25} in MD95-2010 reflect southward migration of the ice edge and marginal ice zone during terminal GI (Fig. 2*A*). This trend culminated in near-perennial sea ice cover in the central Norwegian Sea, severe seasonal sea ice conditions in the southern Norwegian Sea, and breakdown of the large-scale phytoplankton production at GI-GS transitions.

The PIP_{25} records of both cores also consistently reflect the millennial-scale sea ice variability reconstructed from the individual biomarker signals. Increased $P_{III}IP_{25}$ and P_BIP_{25} values of ~0.5–0.9 in core MD95-2010 reflect a strong seasonal to near-perennial sea ice cover for the central Norwegian Sea during GS, while lowered values of ~0.2–0.4 indicate a substantially reduced seasonal sea ice cover or largely open-water conditions during GI (Fig. 3 *A*–*C*). On average, the median, maximum, and minimum PIP_{25} values are larger in MD95-2010 than in MD99-2284. Although being biased in part by different temporal resolutions for GS and GI intervals in both cores, this is consistent with overall more severe sea ice conditions, that is a longer winter sea ice season, in the central Norwegian Sea compared to the southern Norwegian Sea. In turn, a generally longer summer season of open waters in the southern Norwegian Sea may add to brassicasterol values being generally one order of magnitude higher in MD99-2284 than in MD95-2010 (Fig. 2*A*). Also, site MD99-2284 may have been located closer to the glacial Polar Front, where an increased nutrient availability induced enhanced phytoplankton and biomarker production, compared to site MD95-2010 further north under a stronger influence of low-productive polar surface waters. The shift from an extensive stadial to a reduced interstadial sea ice cover appears more rapid in the PIP_{25} records of core MD95-2010, compared to the P_BIP_{25} record of MD99-2284. This may reflect a more gradual initial sea ice retreat in the southern Norwegian Sea during the later parts of GS (24), followed by a rapid sea ice reduction in the central Norwegian Sea at GS-GI transitions.

Sea Ice Proxy Evidence from the RECAP Ice Core. To assist the interpretation of our marine sea ice records, we enhanced the temporal resolution of the RECAP Br_{enr}-based sea ice record between 32 and 41 ka, previously presented at a lower resolution for the last 120 ky (32). The Br_{enr} proxy is based on the bromine-to-sodium mass ratio of ice normalized to that of seawater, and is considered as reflecting first-year (i.e., seasonal) sea ice conditions in the marine aerosol source area (32, 44, 45) (*SI Appendix, Materials and Methods*). Bromine recycling processes occurring over seasonal (first year) sea ice formation add photochemically derived bromine to the sea salt-derived aerosol inventory of the overlying atmosphere, consequently leading to increased Br_{enr} values in snow and ice precipitating nearby (46). Processes associated with aerosol transport and deposition might additionally influence the Br_{enr} signals in ice cores (32, 47). Nevertheless, an enhanced Br_{enr} (>1) in Greenland ice cores is considered to reflect extensive seasonal sea ice in the marine aerosol source area (32, 45). In turn, a lowered ice core Br_{enr} (~1) results from the lack of bromine recycling related to absence or reduced presence of seasonal sea ice, indicating the dominance of either open water or multiyear/perennial sea ice in the source area (32, 45).

For the time period studied, the RECAP Br_{enr} reveals pronounced millennial-scale variability in line with D-O climate cycles, while variations in individual bromine and sodium concentrations are less consistent with the D-O variability (Fig. 3*D* and *SI Appendix*, Fig. S4). Increased RECAP Br_{enr} values of ~8–16 during GS suggest that the northern North Atlantic and Nordic Seas (~50–85°N) were covered by extensive seasonal sea ice (32), which is in agreement with our biomarker results from the Norwegian Sea (Fig. 3). Highest Br_{enr} values occurring during GS9 may reflect the largest spatial extent of seasonal sea ice probably related to Heinrich Event 4, suggesting that winter sea ice might have extended further south into the North Atlantic as compared with other GS. The lowered Br_{enr} values of ~1–5 during GI indicate reduced Br activation from seasonal sea ice surfaces. This could result either from enhanced perennial sea ice or enhanced open-water conditions in the marine aerosol source area. The latter interpretation would agree with our biomarker sea ice reconstruction that reflects enhanced open-ocean conditions and a reduced seasonal sea ice extent in the Norwegian Sea during GI. This interpretation of the RECAP Br_{enr} variability during D-O cycles is consistent with Br_{enr} being increased during the cold Younger Dryas stadial and decreasing into the Holocene, which agrees well with deglacial sea ice reduction reconstructed from marine sea ice records from the Nordic Seas (23, 32, 48).

In contrast to the RECAP ice core, the NEEM (North Greenland Eemian Ice Drilling) ice core from northwestern Greenland shows lowered Br_{enr} values during GS (and the Younger Dryas) and increased Br_{enr} values during GI and the Holocene (45). These Br_{enr} trends in the NEEM ice core, whose aerosol source area comprises the Baffin Bay and Canadian Arctic, have been interpreted as reflecting an extensive perennial/multiyear sea ice cover during GS and a partial replacement of perennial sea ice by seasonal sea ice during GI and the Holocene (45). Hence, while the NEEM Br_{enr} record appears to be controlled by multiyear versus seasonal sea ice in the Baffin Bay, the RECAP Br_{enr} signals may be dominated by the presence of seasonal sea ice versus open water in the northern North Atlantic and Nordic Seas (32). On this basis, we argue that the lowered RECAP Br_{enr} during GI is most likely due to enhanced open-water conditions and reduced seasonal sea ice presence. The glacial millennial-scale variability in sea ice cover reflected by the RECAP Br_{enr} record is thus consistent with our biomarker sea ice reconstruction, suggesting that the northern North Atlantic and the Nordic Seas were extensively covered by seasonal sea ice during GS and characterized by more open-ocean conditions during GI.

Discussion

Our sediment and ice core proxy records reveal with unprecedented coherence and spatial representation the sea ice conditions and in particular the spatial extent of seasonal sea ice cover in the Nordic Seas and northern North Atlantic during GI and GS, as illustrated schematically in Fig. 4. The millennial-scale sea ice variability derived from our sediment and ice core proxy records is in agreement with previous biomarker sea ice reconstructions from the southern Norwegian Sea (23, 24) as well as with trends observed in several model simulations (8, 14, 15). In contrast to our results which are based on coherent responses in biomarker records of separate cores and independent ice core results, dinoflagellate cyst assemblage records from the Norwegian Sea have been interpreted to reflect reduced sea ice formation during GS and longer sea ice cover duration during GI (27–29). These apparently opposing trends in glacial sea ice variability based on biomarker and Br_{enr} records on the one hand and dinoflagellate cyst records on the other might hint at different sensitivity or calibration issues associated with each sea ice proxy, which remains to be investigated in future studies.

We argue that our reconstructed extensive sea ice cover during GS is consistent with a reduced AMOC (19, 20), cooler sea-surface temperatures in the North Atlantic (49, 50), and an enhanced surface stratification and intermediate-water warming in the Nordic Seas

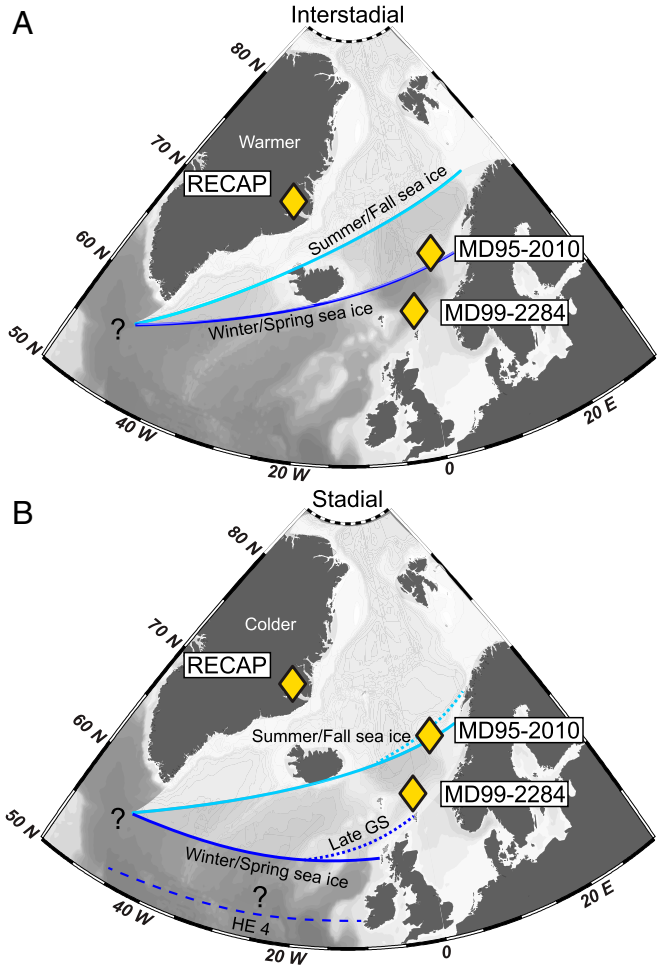

Fig. 4. Schematic of sea ice conditions in the glacial Nordic Seas and North Atlantic. The simplified sea ice cover based on our reconstruction and Greenland temperature trends are shown for (*A*) interstadials and (*B*) stadials. Light-blue lines indicate the summer/fall sea ice extent and dark-blue lines reflect the winter/spring sea ice extent, with the area in between representing the seasonal sea ice cover. The dashed dark-blue line in *B* shows the more extensive winter/spring sea ice extent during Heinrich Event 4 (HE 4). Dotted lines in *B* illustrate the initial sea ice retreat in the southeastern Nordic Seas during late GS. Yellow diamonds mark the core sites investigated in this study. The maps were produced with Ocean Data View software (65).

reflecting the lack of deep-ocean convection (13, 18, 21, 22, 24). This stadial subsurface to deep-water warming is reflected, for example, by decreased benthic foraminiferal $\delta^{18}O$ values in MD95-2010 and MD99-2284 as well as by increased temperatures derived from the benthic foraminiferal Mg/Ca record from MD99-2284 (Fig. 3*E*). While sea ice and oceanographic conditions in the Norwegian Sea were comparable during all GS investigated, the RECAP Br_{enr} record suggests most extensive seasonal sea ice conditions in the North Atlantic for GS9, which may be linked to the pronounced AMOC weakening related to Heinrich Event 4 (19, 20) (Fig. 4*B*). In turn, a reduced seasonal sea ice cover during GI is in accordance with a strengthened AMOC (19, 20), warmer temperatures in the North Atlantic (49, 50), and diminished surface stratification and reinvigorated deep-water formation in the Norwegian Sea, as indicated by deep-water cooling (13, 18, 21, 22, 24) (Fig. 3*E*).

To constrain the timing and duration of the sea ice decline at the abrupt GS-GI transitions we make use of the RECAP ice core chronology, which rests on alignment of the RECAP dust and NGRIP $\delta^{18}O$ and is especially robust at GS-GI transitions where the alignment was centered (37) (Fig. 5 and *SI Appendix*, Fig. S2). Where the drops in RECAP Br_{enr} reflecting large-scale sea ice decline are constrained best, it happens at most within 460 y across the GS9-GI8 transition and within 250 y just prior to or at the GS8-GI7 transitions (Fig. 5 *A* and *B*). Considering that each Br_{enr} values is from an ∼1.5-cm-thick ice core sample, integrating ∼50–130 y, the Br_{enr} decrease at the GS9-GI8 transition might happen within 270 y, corresponding to a 4.8-cm-wide sampling gap (Fig. 5*B*). Only at the GS8-GI7 transition is the Br_{enr} drop recorded between directly adjacent ice core samples, each of which is 1.5 cm thick, corresponding to ∼125 y (Fig. 5*A*). We therefore argue that 250 y may be considered as representative, yet conservative duration estimate for the major GS-GI sea ice decline. However, further high-resolution proxy evidence covering several glacial D-O events is desirable to confirm the short duration of the sea ice decline. Nonetheless, the Br_{enr}-based large-scale sea ice retreat is coeval—in terms of pacing and duration—with the PIP_{25} drop in MD95-2010 reflecting sea ice decline in the central Norwegian Sea, despite a potential smoothing of the sedimentary proxy signals through bioturbation (Fig. 5). This provides credence in the robustness of our sediment core chronology and strongly supports that major sea ice decline in the Nordic Seas happened rapidly, within 250 y or less, just prior to or at the onset of the atmospheric warming of the D-O events recorded by the NGRIP $\delta^{18}O$.

The rapid large-scale sea ice decline in the Nordic Seas matches a rapid ∼2–3 °C overshoot in near-surface temperature and an ∼1‰ increase in benthic $\delta^{18}O$, recorded in MD99-2284 (Fig. 5). The increase in benthic $\delta^{18}O$ probably reflects deep-water cooling by ∼2–3 °C, as supported by independent benthic foraminiferal Mg/Ca-based evidence (21, 22) (Fig. 3*E*). The near-surface temperature overshoot reflects maximum inflow of warm and saline Atlantic surface waters into the Norwegian Sea, while the deep-water cooling suggests deep-ocean convection (21, 22, 24). The concurrence and rapidity of surface and deep-water temperature changes at site MD99-2284 and the major sea ice decline, recorded at site MD95-2010 and in the RECAP ice core, are supported by the tight alignment of rather gradual ARM increases at the GS-GI transitions in both sediment cores. Our results thus testify that the rapid sea ice decline shaped a threshold response of both deep convection in the Nordic Seas and D-O climate transitions in Greenland (9, 10).

The major sea ice decline associated with enhanced northward flow of warm Atlantic surface waters and reinvigorated local deep convection imply rapid and widespread exposure and release of oceanic heat and moisture from the Nordic Seas to the high-latitude atmosphere. This, together with a decrease in albedo, amplified the atmospheric warming of a D-O event (9, 10). Vice versa, seasonal sea ice expansion and reduction of deep convection led to an increased albedo and reduced ocean-atmosphere heat exchange, facilitating the abrupt GI-GS cooling transitions. Moreover, the rapid large-scale demise of seasonal sea ice cover derived from our proxy records would allow for an increased proportion of evaporation and subsequent precipitation during colder months for GI, as compared to GS. This supports a sea ice control of changes in moisture source and precipitation seasonality that may in part be responsible for the large $\delta^{18}O$ amplitudes in Greenland ice cores during D-O cycles (51).

Our proxy data indicate that the rapid GS-GI sea ice decline was preceded by an initial sea ice retreat in the southern Norwegian Sea during late GS (Fig. 4*B*), as evidenced by the IP_{25} and P_BIP_{25} records of MD99-2284 (24). This initial sea ice retreat may be considered as a shortening of the winter sea ice season and prolongation of the summer open-ocean season. It is known from the modern Arctic Ocean that a prolongation of the open-ocean season leads to an increased heat loss from the ocean to the atmosphere (2, 52, 53). This, in turn, results in a strengthening of winter convective surface ocean mixing and can

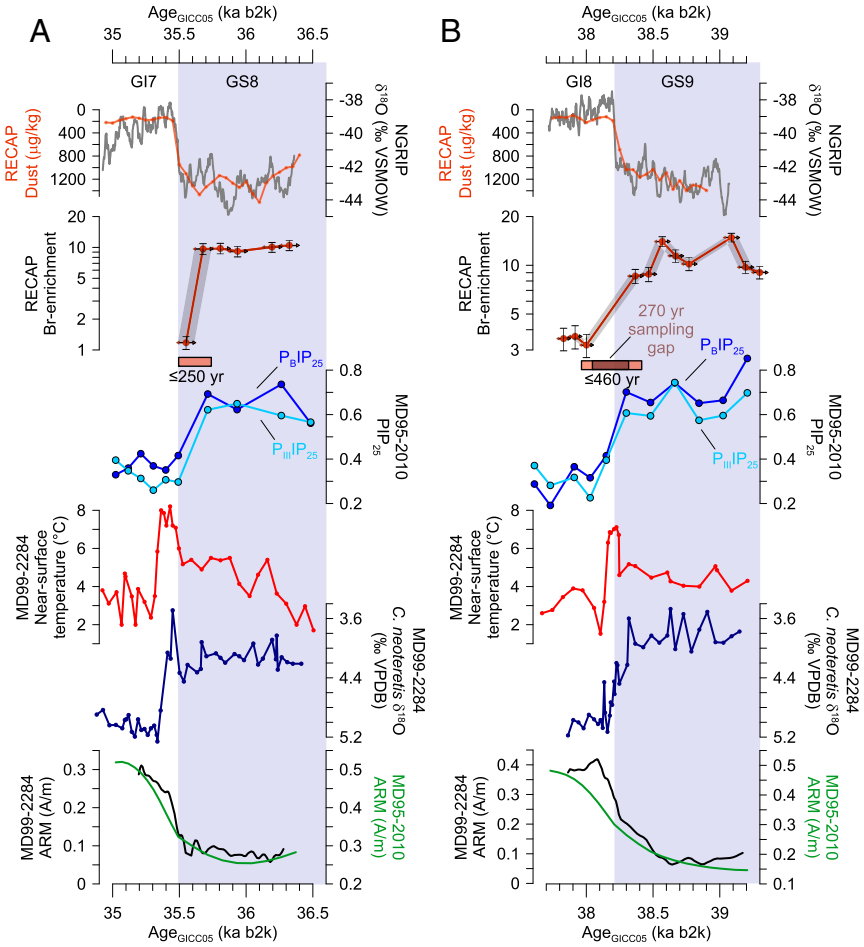

Fig. 5. High-resolution sediment and ice core proxy records covering the GS-GI climate transitions. The records are shown for (*A*) the GS8-GI7 transition at ~35.5 ka and (*B*) the GS9-GI8 transition at ~38.2 ka, and include from top to bottom: $\delta^{18}O$ of the NGRIP ice core plotted as 11-point running average (gray) (6) and dust of the RECAP ice core (orange) (37); Br_{enr} of the RECAP ice core (red) with the maximum duration of the GS-GI sea ice decline and a 270-y sampling gap in *B* indicated; P_BIP_{25} (blue) and $P_{III}IP_{25}$ (light blue) of MD95-2010; Near-sea surface temperature estimates based on planktic foraminifera census counts of MD99-2284 (13); Benthic foraminiferal $\delta^{18}O$ of MD99-2284 (13); ARM (10^{-6} A/m) of MD95-2010 (green) (34, 35) and MD99-2284 (black) (13) showing the good alignment of both cores. All records are plotted on the GICC05 b2k timescale (36). GI and GS (shaded bars) are numbered at the top.

thereby foster further sea ice retreat, as for example observed in the modern Barents Sea (54, 55). By analogy to these observations, we argue that increasing winter heat loss and resulting convective surface mixing in the Norwegian Sea strengthened toward GS-GI transitions, as the seasonal sea ice cover retreated. The seasonal sea ice retreat during late GS may have been confined to the Atlantic inflow region in the southeastern Norwegian Sea, while the wider North Atlantic sea ice cover remained extensive, especially during GS9 comprising Heinrich Event 4 (Fig. 4*B*). The proposed initial retreat in seasonal sea ice cover and associated strengthening of convective activity during late GS could also explain the presence of early warning signals for D-O events, identified as increased variance and autocorrelation in the decadal-scale variability of the Greenland ice core $\delta^{18}O$ (56). This illustrates the threshold behavior of both sea ice cover and ocean convection in the Nordic Seas, with a bifurcation point being reached at GS-GI transitions.

It was previously shown that the initial sea ice retreat in the southern Norwegian Sea during late GS was probably coupled with an enhanced advection of warm and saline surface waters from the North Atlantic (24). This is consistent with glacial model simulations using a freshwater hosing, which also revealed a gradual northward migration and deepening of open-ocean convection in the northern North Atlantic before rapid sea ice decline and abrupt climate change at GS-GI transitions (4, 14, 24). Moreover, planktic and benthic foraminiferal radiocarbon evidence from core MD99-2284 points at a strengthening of ocean convection accompanied by sea ice retreat in the southern Norwegian Sea during the deglaciation, preceding the abrupt climate change of the Bølling-Allerød interstadial by ~400 y (48). All this supports that thermohaline circulation changes in the northern North Atlantic or other changes in the northward extent of the upper limb of the AMOC may have led to the sea ice decline at GS-GI transitions (8–10, 14). Similar to this glacial scenario, the observed sea ice reduction in parts of the modern Arctic has been linked with a strengthening and warming of the Atlantic inflow (57, 58), although anthropogenically altered radiative forcing is likely an additional forcing of today's sea ice demise (59).

Changes in thermohaline circulation and sea ice cover in the Nordic Seas may have resulted from changes in winds and the subpolar gyre circulation in the glacial North Atlantic (60). A steady and southward-shifted North Atlantic jet stream during GS would have maintained a fresh and cold North Atlantic, a reduced subpolar gyre circulation, and weakened northward ocean heat transport, fostering an extensive sea ice cover (60). A change toward a northward-shifted jet and generally stronger winds over the North Atlantic would have forced a more

vigorous subpolar gyre circulation and enhanced ocean heat transport to the Norwegian Sea, leading to sea ice reduction (60). It has also been suggested that thermohaline convective instability beneath the stadial sea ice cover, resulting from subsurface warming and surface salinity changes, might have led to an abrupt sea ice decline and Greenland warming (15, 25, 26). It appears that, rather than a sole trigger, coupled atmosphere–sea ice–ocean dynamics in the subpolar North Atlantic, acting in a feedback loop under glacial boundary conditions, may have produced the D-O climate variability (60). Our proxy records and interpretation suggest that various coupled atmospheric–sea ice–ocean changes may have shifted gradually and led up to a threshold response in sea ice cover and deep convection in the Nordic Seas.

In conclusion, our study provides unprecedentedly detailed, spatially coherent, and temporally constrained and consistent empirical evidence that resolves rapid large-scale sea ice decline in the Nordic Seas occurring concomitantly with the glacial D-O events, after an initial seasonal sea ice reduction in the southern Norwegian Sea. Our results thus strongly support that rapid sea ice decline and associated positive feedbacks shaped the transition from surface stratification to deep ocean convection in the Nordic Seas and acted as critical tipping element that amplified and possibly initiated the abrupt D-O climate change (10, 61). Our findings also raise questions as to whether the currently observed Arctic sea ice decline will lead to a similar destabilization of surface stratification and to what extent this will further amplify climate warming in the Arctic (2, 4, 55, 62).

Methods

Age models of cores MD95-2010 and MD99-2284 are based on stratigraphic alignment of marine proxy records and the NGRIP $\delta^{18}O$ record, using signals in ARM, near-surface temperature, and cryptotephra layers (*SI Appendix, Materials and Methods*). Biomarkers were extracted from freeze-dried and homogenized sediment samples using dichloromethane:methanol (2:1, vol/vol) as solvent, separated into hydrocarbon and sterol fractions, and analyzed by gas chromatography/mass spectrometry. Bromine and sodium contents in RECAP ice core samples were analyzed by collision reaction cell-inductively coupled plasma-mass spectrometry. Further methodological details are provided in *SI Appendix, Materials and Methods*.

Data Availability. All proxy data presented in this study are available in Datasets S1–S7. All study data are included in the article and *SI Appendix*.

ACKNOWLEDGMENTS. We thank the IMAGES program and R/V Marion Dufresne crews and scientific parties on legs MD101 and MD114, and Walter Luttmer for assistance with biomarker analyses. We are also grateful to the RECAP ice coring effort, which was financed by the Danish Research Council through a Sapere Aude grant, the NSF through the Division of Polar Programs, and the Alfred Wegener Institute. The research leading to these results has received funding to the ice2ice project from the European Research Council (ERC) Synergy Grant under the European Union's Seventh Framework Programme (FP7/2007-2013)/ERC Grant Agreement 610055. We thank three anonymous reviewers for their constructive comments that helped to improve the manuscript.

1. G. S. Dieckmann, H. H. Hellmer, The importance of sea ice: An overview. *Sea Ice* **2**, 1–22 (2010).
2. J. A. Screen, I. Simmonds, The central role of diminishing sea ice in recent Arctic temperature amplification. *Nature* **464**, 1334–1337 (2010).
3. J. Stroeve, M. M. Holland, W. Meier, T. Scambos, M. Serreze, Arctic sea ice decline: Faster than forecast. *Geophys. Res. Lett.* **34**, L09501 (2007).
4. E. Jansen *et al.*, Past perspectives on the present era of abrupt Arctic climate change. *Nat. Clim. Chang.* **10**, 714–721 (2020).
5. W. Dansgaard *et al.*, Evidence for general instability of past climate from a 250-kyr ice-core record. *Nature* **364**, 218–220 (1993).
6. K. K. Andersen *et al.*; North Greenland Ice Core Project members, High-resolution record of Northern Hemisphere climate extending into the last interglacial period. *Nature* **431**, 147–151 (2004).
7. P. Kindler *et al.*, Temperature reconstruction from 10 to 120 kyr b2k from the NGRIP ice core. *Clim. Past* **10**, 887–902 (2014).
8. A. Ganopolski, S. Rahmstorf, Rapid changes of glacial climate simulated in a coupled climate model. *Nature* **409**, 153–158 (2001).
9. A. Timmermann, H. Gildor, M. Schulz, E. Tziperman, Coherent resonant millennial-scale climate oscillations triggered by massive meltwater pulses. *J. Clim.* **16**, 2569–2585 (2003).
10. H. Gildor, E. Tziperman, Sea-ice switches and abrupt climate change. *Philos. Trans. R. Soc. Lond. Math. Phys. Eng. Sci.* **361**, 1935–1942, discussion 1942–1944 (2003).
11. C. Li, D. S. Battisti, D. P. Schrag, E. Tziperman, Abrupt climate shifts in Greenland due to displacements of the sea ice edge. *Geophys. Res. Lett.* **32**, L19702 (2005).
12. C. Li, D. S. Battisti, C. M. Bitz, Can North Atlantic sea ice anomalies account for Dansgaard–Oeschger climate signals? *J. Clim.* **23**, 5457–5475 (2010).
13. T. M. Dokken, K. H. Nisancioglu, C. Li, D. S. Battisti, C. Kissel, Dansgaard-Oeschger cycles: Interactions between ocean and sea ice intrinsic to the Nordic seas. *Paleoceanogr. Paleoclimatol.* **28**, 491–502 (2013).
14. L. Menviel, A. Timmermann, T. Friedrich, M. H. England, Hindcasting the continuum of Dansgaard–Oeschger variability: Mechanisms, patterns and timing. *Clim. Past* **10**, 63–77 (2014).
15. G. Vettoretti, W. R. Peltier, Thermohaline instability and the formation of glacial North Atlantic super polynyas at the onset of Dansgaard-Oeschger warming events. *Geophys. Res. Lett.* **43**, 5336–5344 (2016).
16. B. Hansen, S. Østerhus, North Atlantic–Nordic seas exchanges. *Prog. Oceanogr.* **45**, 109–208 (2000).
17. B. Rudels *et al.*, "Observations in the ocean" in *Arctic Climate Change: The ACSYS Decade and Beyond*, P. Lemke, Ed. (Springer, 2012), pp. 117–198.
18. T. L. Rasmussen, E. Thomsen, The role of the North Atlantic Drift in the millennial timescale glacial climate fluctuations. *Palaeogeogr. Palaeoclimatol. Palaeoecol.* **210**, 101–116 (2004).
19. E. Böhm *et al.*, Strong and deep Atlantic meridional overturning circulation during the last glacial cycle. *Nature* **517**, 73–76 (2015).
20. L. G. Henry *et al.*, North Atlantic ocean circulation and abrupt climate change during the last glaciation. *Science* **353**, 470–474 (2016).
21. M. M. Ezat, T. L. Rasmussen, J. Groeneveld, Persistent intermediate water warming during cold stadials in the southeastern Nordic seas during the past 65 ky. *Geology* **42**, 663–666 (2014).
22. E. G. Sessford *et al.*, Consistent fluctuations in intermediate water temperature off the coast of Greenland and Norway during Dansgaard-Oeschger events. *Quat. Sci. Rev.* **223**, 105887 (2019).
23. U. Hoff, T. L. Rasmussen, R. Stein, M. M. Ezat, K. Fahl, Sea ice and millennial-scale climate variability in the Nordic seas 90 kyr ago to present. *Nat. Commun.* **7**, 12247 (2016).
24. H. Sadatzki *et al.*, Sea ice variability in the southern Norwegian Sea during glacial Dansgaard-Oeschger climate cycles. *Sci. Adv.* **5**, eaau6174 (2019).
25. M. F. Jensen, J. Nilsson, K. H. Nisancioglu, The interaction between Sea ice and salinity-dominated ocean circulation: Implications for halocline stability and rapid changes of sea ice cover. *Clim. Dyn.* **47**, 3301–3317 (2016).
26. M. F. Jensen, K. H. Nisancioglu, M. A. Spall, Large changes in sea ice triggered by small changes in Atlantic water temperature. *J. Clim.* **31**, 4847–4863 (2018).
27. F. Eynaud *et al.*, Norwegian sea-surface palaeoenvironments of marine oxygen-isotope stage 3: The paradoxical response of dinoflagellate cysts. *J. Quat. Sci. Publ. Quat. Res. Assoc.* **17**, 349–359 (2002).
28. M. Wary *et al.*, Norwegian Sea warm pulses during Dansgaard-Oeschger stadials: Zooming in on these anomalies over the 35–41 ka cal BP interval and their impacts on proximal European ice-sheet dynamics. *Quat. Sci. Rev.* **151**, 255–272 (2016).
29. M. Wary *et al.*, Regional seesaw between the North Atlantic and Nordic Seas during the last glacial abrupt climate events. *Clim. Past* **13**, 729–739 (2017).
30. J. Müller, R. Stein, High-resolution record of late glacial and deglacial sea ice changes in Fram Strait corroborates ice–ocean interactions during abrupt climate shifts. *Earth Planet. Sci. Lett.* **403**, 446–455 (2014).
31. A. Kremer *et al.*, A 190-ka biomarker record revealing interactions between sea ice, Atlantic water inflow and ice sheet activity in eastern Fram Strait. *Arktos* **4**, 22 (2018).
32. N. Maffezzoli *et al.*, A 120 000-year record of sea ice in the North Atlantic? *Clim. Past* **15**, 2031–2051 (2019).
33. S. M. P. Berben *et al.*, Independent tephrochronological evidence for rapid and synchronous oceanic and atmospheric temperature rises over the Greenland stadial-interstadial transitions between ca. 32 and 40 ka b2k. *Quat. Sci. Rev.* **236**, 106277 (2020).
34. C. Kissel *et al.*, Rapid climatic variations during marine isotopic stage 3: Magnetic analysis of sediments from Nordic seas and North Atlantic. *Earth Planet. Sci. Lett.* **171**, 489–502 (1999).
35. T. M. Dokken, E. Jansen, Rapid changes in the mechanism of ocean convection during the last glacial period. *Nature* **401**, 458–461 (1999).
36. K. K. Andersen *et al.*, The Greenland ice core chronology 2005, 15–42 ka. Part 1: Constructing the time scale. *Quat. Sci. Rev.* **25**, 3246–3257 (2006).
37. M. F. Simonsen *et al.*, East Greenland ice core dust record reveals timing of Greenland ice sheet advance and retreat. *Nat. Commun.* **10**, 4494 (2019).
38. S. T. Belt *et al.*, A novel chemical fossil of paleo sea ice: IP25. *Org. Geochem.* **38**, 16–27 (2007).
39. S. T. Belt *et al.*, Identification of paleo Arctic winter sea ice limits and the marginal ice zone: Optimised biomarker-based reconstructions of late quaternary Arctic sea ice. *Earth Planet. Sci. Lett.* **431**, 127–139 (2015).
40. L. Smik, P. Cabedo-Sanz, S. T. Belt, Semi-quantitative estimates of paleo Arctic sea ice concentration based on source-specific highly branched isoprenoid alkenes: A further development of the PIP25 index. *Org. Geochem.* **92**, 63–69 (2016).

41. J. K. Volkman, A review of sterol markers for marine and terrigenous organic matter. *Org. Geochem.* **9**, 83–99 (1986).
42. J. Müller *et al*., Towards quantitative sea ice reconstructions in the northern North Atlantic: A combined biomarker and numerical modelling approach. *Earth Planet. Sci. Lett.* **306**, 137–148 (2011).
43. X. Xiao, K. Fahl, J. Müller, R. Stein, Sea-ice distribution in the modern Arctic Ocean: Biomarker records from trans-Arctic Ocean surface sediments. *Geochim. Cosmochim. Acta* **155**, 16–29 (2015).
44. A. Spolaor *et al*., Sea ice dynamics influence halogen deposition to Svalbard. *Cryosphere* **7**, 1645–1658 (2013).
45. A. Spolaor *et al*., Canadian Arctic sea ice reconstructed from bromine in the Greenland NEEM ice core. *Sci. Rep.* **6**, 33925 (2016).
46. A. Spolaor *et al*., Seasonality of halogen deposition in polar snow and ice. *Atmos. Chem. Phys.* **14**, 9613–9622 (2014).
47. K. A. Pratt *et al*., Photochemical production of molecular bromine in Arctic surface snowpacks. *Nat. Geosci.* **6**, 351–356 (2013).
48. F. Muschitiello *et al*., Deep-water circulation changes lead North Atlantic climate during deglaciation. *Nat. Commun.* **10**, 1272 (2019).
49. S. Van Kreveld *et al*., Potential links between surging ice sheets, circulation changes, and the Dansgaard-Oeschger cycles in the Irminger Sea, 60–18 kyr. *Paleoceanography* **15**, 425–442 (2000).
50. M. F. Jensen *et al*., A spatiotemporal reconstruction of sea-surface temperatures in the North Atlantic during Dansgaard–Oeschger events 5–8. *Clim. Past* **14**, 901–922 (2018).
51. L. C. Sime, P. O. Hopcroft, R. H. Rhodes, Impact of abrupt sea ice loss on Greenland water isotopes during the last glacial period. *Proc. Natl. Acad. Sci. U.S.A.* **116**, 4099–4104 (2019).
52. S. Manabe, R. J. Stouffer, Two stable equilibria of a coupled ocean-atmosphere model. *J. Clim.* **1**, 841–866 (1988).
53. J. Boé, A. Hall, X. Qu, September sea-ice cover in the Arctic Ocean projected to vanish by 2100. *Nat. Geosci.* **2**, 341–343 (2009).
54. I. V. Polyakov *et al*., Winter convection transports Atlantic water heat to the surface layer in the eastern Arctic Ocean. *J. Phys. Oceanogr.* **43**, 2142–2155 (2013).
55. S. Lind, R. B. Ingvaldsen, T. Furevik, Arctic warming hotspot in the northern Barents Sea linked to declining sea-ice import. *Nat. Clim. Chang.* **8**, 634–639 (2018).
56. N. Boers, Early-warning signals for Dansgaard-Oeschger events in a high-resolution ice core record. *Nat. Commun.* **9**, 2556 (2018).
57. R. F. Spielhagen *et al*., Enhanced modern heat transfer to the Arctic by warm Atlantic Water. *Science* **331**, 450–453 (2011).
58. M. Årthun, T. Eldevik, L. H. Smedsrud, Ø. Skagseth, R. B. Ingvaldsen, Quantifying the influence of Atlantic heat on Barents Sea ice variability and retreat. *J. Clim.* **25**, 4736–4743 (2012).
59. D. Notz, J. Stroeve, Observed Arctic sea-ice loss directly follows anthropogenic CO2 emission. *Science* **354**, 747–750 (2016).
60. C. Li, A. Born, Coupled atmosphere-ice-ocean dynamics in Dansgaard-Oeschger events. *Quat. Sci. Rev.* **203**, 1–20 (2019).
61. W. S. Broecker, Abrupt climate change: Causal constraints provided by the paleoclimate record. *Earth Sci. Rev.* **51**, 137–154 (2000).
62. I. V. Polyakov *et al*., Greater role for Atlantic inflows on sea-ice loss in the Eurasian basin of the Arctic Ocean. *Science* **356**, 285–291 (2017).
63. A. Navarro-Rodriguez, S. T. Belt, J. Knies, T. A. Brown, Mapping recent sea ice conditions in the Barents Sea using the proxy biomarker IP25: Implications for palaeo sea ice reconstructions. *Quat. Sci. Rev.* **79**, 26–39 (2013).
64. F. Fetterer, K. Knowles, W. Meier, M. Savoie, A. K. Windnagel, Sea Ice Index, Version 3 (NSIDC National Snow Ice Data Center, Boulder, CO, 2017).
65. R. Schlitzer, Ocean data view (2017). https://odv.awi.de/. Accessed 6 February 2017.